Theor Appl Genet (2014) 127:831–841
DOI 10.1007/s00122-014-2260-8

ORIGINAL PAPER

# Fine mapping and metabolic and physiological characterization of the glume glaucousness inhibitor locus *Iw3* derived from wild wheat

**Jing Wang · Wanlong Li · Wei Wang**

Received: 10 August 2013 / Accepted: 3 January 2014 / Published online: 13 February 2014


**Abstract**
***Key message*** **This research provided the first view of metabolic and physiological effect of a tissue-specific glaucousness inhibitor in wheat and laid foundation for map-based cloning of the *Iw3* locus.**
*Abstract* Cuticular wax constitutes the outermost layer of plant skin, and its composition greatly impacts plant appearance and plant–environment interaction. Epicuticular wax in the upper part of adult wheat plants can form the glaucousness, which is associated with drought tolerance. In this research, we characterized a glume-specific glaucousness inhibitor, *Iw3*, by fine mapping, physiological, and molecular approaches. *Iw3* inhibits glaucousness formation by altering wax composition. Compared to the wild type, *Iw3* eliminated β-diketone, reduced 47 % primary alcohols, but increased aldehyde 400-fold and alkanes fivefold, which led to 30 % reduction of total glume wax load. Loss of the glaucousness increased cuticle permeability, suggesting an important role in drought sensitivity. Genetically, the glaucousness-inhibiting effect by *Iw3* is partially dominant in a dosage-dependent manner. We localized the *Iw3* locus within a 0.13-cM interval delimited by marker loci *Xpsp3000* and *XWL3096*. Of the 53 wax genes assayed, we detected transcription changes in nine genes by *Iw3*, downregulation of *Cer4-1* and upregulation of other five *Cer4* and three *KCS* homologs. All these results provided initial insights into *Iw3*-mediated regulation of wax metabolism and paved way for in-depth characterization of the *Iw3* locus and the glaucousness-related β-diketone pathway.

Communicated by I. D. Godwin.

**Electronic supplementary material** The online version of this article (doi:10.1007/s00122-014-2260-8) contains supplementary material, which is available to authorized users.

J. Wang
College of Agronomy, Northwestern A&F University, Yangling 712100, Shaanxi, China

J. Wang · W. Li (✉) · W. Wang
Department of Biology and Microbiology, South Dakota State University, Brookings, SD 57007, USA
e-mail: wanlong.li@sdstate.edu

W. Li
Department of Plant Science, South Dakota State University, Brookings, SD 57007, USA

## Introduction

Drought has long been a major threat to global crop production, and climate change exaggerates its scale and frequency. The recent drought waves represent alarms to the future agriculture and call for a much-needed "Blue Revolution" to increase water use efficiency (WUE) (Pennisi 2008). Physiologically, reducing transpiration rate is an effective mechanism for enhancing plant tolerance to drought and increasing WUE. Two types of transpirations have been recognized: stomatal and nonstomatal. While stomatal transpiration regulation depends upon sophisticated signal transduction and ion channel operation (Shimazaki et al. 2007), the nonstomatal transpiration is protected by an extracellular deposition of cuticle that covers the epidermis of the aboveground organs of land plants. As a barrier between plants and their environment, the cuticle also functions in defending plants against the biotic and other attacks, such as heat and UV (Shepherd and Wynne Griffiths 2006). Structurally, cuticle consists of the cell wall-bound insoluble cutin proper as the foundation and soluble wax inserted in and overlaid on the cutin framework (Samuels et al. 2008). The densely distributed wax

crystals can give plants the white-bluish appearance called bloom or glaucousness.

Cuticular waxes are a mixture of very long chain fatty acids (VLCFAs, chain length ranging from $C_{20}$ to $C_{36}$) and their derivatives including alcohols, aldehydes, alkanes, ketones, and wax esters. The VLCFAs are synthesized by fatty acyl elongase complex using plastid-born $C_{16}$ and $C_{18}$ de novo fatty acids as substrates. The resulting VLCFAs can be reduced to corresponding primary alcohols, which can further be esterified with $C_{16}$ de novo fatty acid into wax esters, in the reduction branch (Vioque and Kolattukudy 1997), or be converted into alkanes (Cheesbrough and Kolattukudy 1984), secondary alcohols, and ketones (Greer et al. 2007) in the decarbonylation branch. The waxes are synthesized in endoplasmic reticulum and transported extracellularly for cuticle formation (Pighin et al. 2004). Tremendous progress has been made in understanding the acyl pathway, including acyl elongation, reduction, and decarbonylation, in the model plant Arabidopsis with many genes for wax synthesis, export, and regulation identified (reviewed in Bernard and Joubès 2013; Lee and Suh 2013; Samuels et al. 2008). This laid a solid foundation for developing cuticle-based strategies to enhance plant drought tolerance.

While this acyl pathway is ubiquitous in the $C_3$ and $C_4$ plants, another parallel pathway is only found in some $C_3$ plants, including the Triticeae crops barley, rye, and wheat, for biosynthesis of hentriacotane-14, 16-dione (β-diketone) and its hydroxy isomers (Bianchi 1995). In common wheat (*Triticum aestivum* L.), the acyl pathway is active in the seedling (vegetative growth) stage, but the β-diketone pathway predominates in the adult plant (reproductive development) stage (Tulloch 1973). Based on biochemical and genetic studies in barley, it was proposed that β-diketone pathway contains chain extension, decarbonylation, and hydroxylation steps, which are defined by mutants of *cer-q*, *cer-c* and *cer-u*, respectively (von Wettstein-Knowles 1995, 2012). Molecular evidence, however, is needed to support this proposed pathway because no gene has been identified for β-diketone synthesis.

Glaucousness is a classical trait in wheat genetic studies. In polyploid wheat, five loci control the glaucousness variations, of which *W1* and *W2* are required for glaucousness formation, but *Iw1*, *Iw2* and *Iw3* for glaucousness inhibition. *W1* and *Iw1* are located on the short arm of chromosome 2B (2BS), *W2* and *Iw2* on 2DS (Tsunewaki and Ebana 1999), and *Iw3*, derived from wild emmer (*T. turgidum* subsp. *dicoccoides*), is located on 1BS (Dubcovsky et al. 1997). The *Iw* gene loci were localized by molecular markers (Adamski et al. 2013; Dubcovsky et al. 1997; Liu et al. 2006; Nelson et al. 1995; Simmonds et al. 2007). In addition to the *W* and *Iw* genes, a quantitative trait locus on chromosome 3A (*QW.aww-3A*) accounts for up to 52 % of genetic variance of flag leaf glaucousness (Bennett et al. 2012). Recent study on a set of glaucousness near isogenic lines (NILs) in common wheat showed that *W1* and *W2* function redundantly in β-diketone synthesis, but their interaction is required for β-diketone hydroxylation, and that *Iw1* and *Iw2* block β-diketone pathway and shunt the metabolites to the acyl reduction branch of the acyl pathway (Zhang et al. 2013). Based on the phenotype, *W1*, *W2*, *Iw1* and *Iw2* are expressed in leaf blades, sheaths and whole spike, but glaucousness-inhibiting effect by the *Iw3* locus is confined to spike (Dubcovsky et al. 1997). This makes *Iw3* unique in tissue specificity of wax regulation and protection of developing seeds from abiotic stresses. We characterized the *Iw3* locus by fine-scale linkage mapping, metabolite profiling of wax components, graphing of wax morphology by scanning electron microscope (SEM), transcription profiling of wax genes by real-time quantitative PCR (qPCR), and evaluating its effect on cuticle permeability. Here we report the results and their implications to wheat drought tolerance.

## Materials and methods

### Plant material and growth conditions

A population of 93 recombinant substitution lines (RSLs) was previously developed from a cross between durum (*T. turgidum* subsp. *durum* (Desf.) Husnot) cv Langdon (LDN) and LDN-*T. turgidum* subsp. *dicoccoides* cv IsA 1B substitution line (LDN-TDIC 1B) by Joppa and Cantrell (1990). The seeds of RSL population, LDN and LDN-TDIC 1B were provided by Dr. Justin Faris (USDA-ARS, Fargo). We repeated the cross and generated a population of 114 $F_2$ individuals. A large population of 3,360 $F_3$ plants was derived from 57 $F_2$ individuals heterozygous at the *Iw3* locus and the flanking marker loci. A pair of *Iw3* NILs was also developed by consecutive selfing of the *Iw3iw3* heterozygous plants and selecting the *Iw3Iw3* and *iw3iw3* homozygotes at $F_6$ generation based on phenotypes and marker genotypes. The RSL and the $F_2$ populations were planted in 10 × 10 cm square pots containing Sunshine® Container Potting Mix 3 (Sun Gro Horticulture) and supplied with Multicote® 8 Controlled-Release Fertilizer (Haifa) in a greenhouse room. Seeds of the $F_3$ population were planted in RooTrainers (Beaver Plastics Ltd), and the recombinants were transplanted into 10 × 10 cm pots. Day length of the greenhouse room was 16 h, and temperatures were 22 °C at day and 18 °C at night. At Feekes' stage (Large 1954) 10.5.1 (F10.5.1), wheat plants are flowering, and we phenotyped the mapping populations by visualizing the glaucousness (Fig. 1).


**Fig. 1** Spikes of *Iw3*-dependent NILs. Their genotypes are indicated underneath each spike. The *scale bar* indicates 1 cm

## PCR genotyping and map construction

DNA was isolated from the parents and segregation populations as described by (Li et al. 2008). Polymerase chain reaction (PCR) was set up in 10 μl containing 100 ng of template DNA, 1 μM primers, 250 μM dNTPs, 1× GoTaq® Reaction Buffer (Promega), and 0.1 U *Taq* polymerase. PCR primers are listed in Supplementary Table 1 s. PCR products were separated by electrophoresis in 2 % agarose gels and 6 % nondenaturing polyacrylamide gels, stained with ethidium bromide (Bio-Rad) and visualized using a U:Genius Gel Imaging System (SYNGene). For the cleaved amplified polymorphic sequence (CAPS) markers, PCR products were digested with appropriate restriction enzymes before gel electrophoresis.

Mapmaker version 3.0 (Lander et al. 1987) was used to determine the marker-gene order and estimate recombination between the marker loci and the *Iw3* locus. An LOD score of 3.0 is applied to all marker loci. The Kosambi (1944) mapping function was used to convert the recombination into genetic distance in terms of Centi-Morgan (cM).

## Scanning electron microscopy (SEM)

For SEM imaging of cuticle surfaces, the glumes were collected from middle positions of spikes at stage F10.5.1. The protocols described by Zhang et al. (2013) were followed for sample pretreatments including replacing the cellular water with glycerol and coating the surface with gold powders. The gold-coated samples were screened with a Hitachi S-3400 N SEM (Hitachi) and images were captured with the voltage set at 5 kV.

## Wax purification and profiling

Glumes were detached from spikes the *Iw3* NILs at stage F10.5.1 for wax extraction. Wax extraction and purification were performed following the protocol described in Zhang et al. (2013). Wax silylation, gas chromatography–mass spectrometry (GC–MS) profiling, and substance identification were performed at the W.M. Keck Metabolomics Research Laboratory of Iowa State University (Ames, IA) on a fee-for-service basis. The wax-extracted glumes were dried at 37 °C for a week and weighed. Five biological replicates were included for each genotype.

## Transcription quantification

At stage F10.1 when awns are visible and heads are emerging from the slit of the flag leaf sheath, we extracted total RNA from glumes using Trizol® reagent (Invitrogen) following the manufacturer's instruction. Approximately 1 μg of total RNA was used for cDNA synthesis in a 20-μl reaction using QuantiTect Rev Transcription Kit (Qiagen), and ~5 ng of cDNA was applied as template for qPCR with a volume of 20 μl. The qPCR primers were adopted from Zhang et al. (2013), and the specificity of each qPCR primer pair was confirmed by melt curve analysis. The qPCR was conducted in 96-well plates with ABI 7900HT High-Throughput Real-Time Themocycler (Life Technologies) using the iTaq™ Fast SYBR® Green Supermix with ROX (Bio-Rad). Two technical and four biological replicates were applied for each of the two NILs. *TaRPII36* was used as an internal reference, and the relative quantities of each amplified product were calculated using the $2^{-\Delta\Delta CT}$ method (Livak and Schmittgen 2001).

## Quantification of cuticle traits

The glumes were detached from spikes of the NIL pair at stage F10.5.1 to evaluate cuticle permeability in terms

of water loss and chlorophyll efflux rate. The samples were dehydrated for 12 h at room temperature (23 °C) and a relative humidity of 44 %. During this process, they were weighed every hour using an AB54-S/FACT analytical balance (Mettler Toledo) with an accuracy of ±0.0001 g. For measuring chlorophyll leaching, glumes from each spike were placed in a 50 ml tube containing 25 ml 80 % ethanol, which were gently agitated on a rotator at 60 rpm. An aliquot of 150 μL supernatant was transferred into a well in a microplate well for quantification and then returned into same tube every hour. After 12 h, the samples were inspected at daily basis for 2 days. The absorbance of supernatant was determined by spectra at 664 and 647 nm using a Synergy 2 Multi-Mode Microplate Reader (Biotek), and total micromolar concentration was calculated as described by Lolle et al. (1997). After the last measurement, the glume samples were dried at 37 °C for 72 h, and the dry weight (DW) was used to calculate the relative rate of water loss and chlorophyll efflux. Two technical and eight biological replicates were included in each genotype for both experiments.

### Data analysis and statistics

Average and standard deviation were calculated from the biological replicates. Student's *t* tests were performed to evaluate the significance of difference between the *Iw3Iw3* and *iw3iw3* homozygotes in wax composition, chlorophyll leaching rate, and water loss rate. Chi squared tests were used to examine if the glaucousness trait segregations in the mapping populations fit the expectation ratios. These tests were carried out using the Excel functions, and cutoff of the *P* values was 0.05.

## Results

### *Iw3* phenotype

Observation of the parental lines, NILs, and segregating populations confirmed that glaucousness-inhibiting effect of *Iw3* is glume-specific. At the same time, we found that *Iw3* is partially dominant because the *Iw3iw3* heterozygote is intermediate (Fig. 1). It resembles those of nonglaucous parent LDN-TDIC 1B and *Iw3Iw3* homozygote from the spikelet-side view, but resembles the glaucous parent LDN and *iw3iw3* homozygote from the spikelet-facing view with a lower intensity of glaucousness (Fig. 1). This was corroborated by genotyping with the cosegregating markers, progeny analysis, and wax morphology under SEM (see below). This feature of *Iw3* facilitates to phenotype the $F_2$ and $F_3$ populations.

### Marker development

Previously *Iw3* was colocalized with the gliadin-coding gene *Gli-B1* in the distal region of chromosome arm 1BS based on restriction fragment length polymorphism (RFLP) genotyping of the 93 RSLs (Dubcovsky et al. 1997). Considering the low map resolution and intractability of RFLP genotyping, we started this project by adopting and developing PCR-based markers. We first selected 33 simple sequence repeat (SSR) markers from the *Gli-B1* region and screened polymorphisms between the two parents. Of these 33 SSR markers, four are polymorphic and used to genotype the RSL population. These include psp3000 from gene *Gli-B1* (Devos et al. 1995), and wmc619, wmc798, and gwm264 from wheat genomic sequences (Röder et al. 1998; Somers et al. 2004). The *Xpsp3000* cosegregated with *Iw3*, and *Xwmc798*, *Xwmc619*, and *Xgwm264* were mapped to positions proximal to the *Iw3* locus (Fig. 2a). In addition to the storage protein-coding genes, this genomic region also harbors several disease resistance genes including *Snn1* and homologs of *Lr21*, and a high density genetic map was constructed encompassing the *Snn1* locus (Reddy et al. 2008). From the *Snn1* map, we selected 13 sequence tagged site (STS) markers, but only fcp618 was polymorphic and amplified a fragment in LDN, not in LDN-TDIC 1B. It also cosegregated with the *Iw3* in the RSL population. For the monomorphic markers, their PCR products were digested with restriction enzymes with 4-base recognition sequences for developing CAPS markers. WL1975, *Rsa* I digestion of PCR amplicon of EST BE406450, detected a codominant polymorphism and mapped 2.1 cM proximal to the *Iw3* locus. We also developed markers directly from the 1BS genomic sequences for the genes or ESTs located in the collinear regions of 1AS and 1DS. Marker WL1967 was developed from the 1BS copy of gene *Lr21*, and markers WL1987, WL2282, and WL3096 were developed from the 1BS genes homologous to ESTs BE496996, BE494877, and BE498831, respectively. While psp3000 and WL2282 are codominant, fcp168, WL1967, WL1987 and WL3096 are dominant markers. They all cosegregated with the *Iw3* locus in the RSL population. As a result, a total of 10 markers were polymorphic between the two parental lines, mapped to the *Iw3* region, and spanned an interval of 8.4 cM (Fig. 2a).

### Fine mapping of *Iw3*

The same markers were also used to genotype the $F_2$ population, which segregated into 23 (*Iw3Iw3*) : 55 (*Iw3iw3*) : 36 (*iw3iw3*), fitting the 1:2:1 ratio ($P = 0.26714$). *XWL2282* was mapped 1.8 cM distal to the *Iw3* locus, but the order of other marker loci remained the same although genetic distances varied. Therefore, marker loci *XWL2282* and *XWL1975* delimit the *Iw3* interval (Fig. 2b).

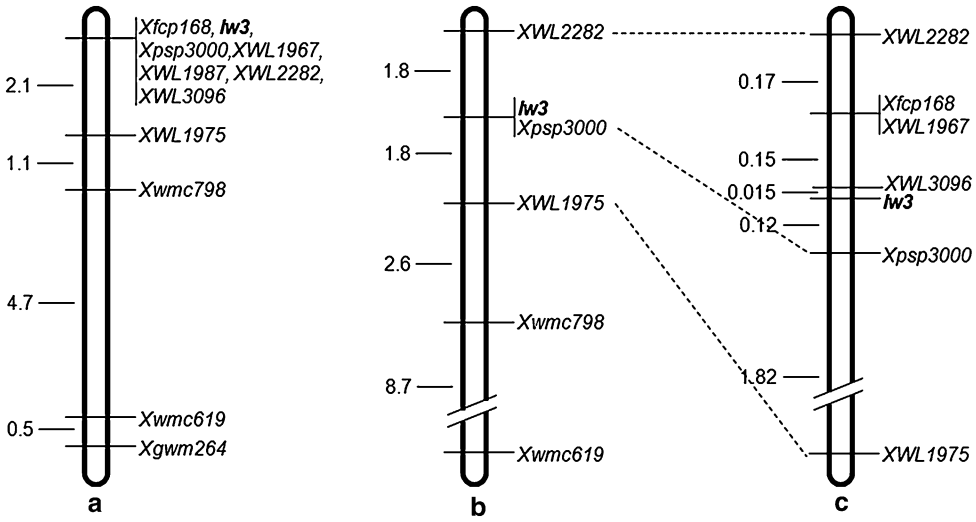


**Fig. 2** Molecular mapping of the *Iw3* locus on the chromosome arm 1BS. **a** A linkage map based on 93 RSLs. **b** A linkage map constructed from 114 $F_2$ individuals. **c** A fine-scale map of the *Iw3* interval constructed based on 3,360 $F_{2:3}$ plants. The marker loci are listed at the *right side* of the maps, and genetic distances (cM) between the marker loci are indicated at the *left side* of the maps. The *Iw3* locus is indicated in *bold*. The *top* of the maps is toward the telomere, and the *bottom* is toward the centromere

From 57 $F_2$ individuals heterozygous at the *Iw3* locus, we generated a large $F_3$ population and started fine mapping of *Iw3* by screening this population using the codominant flanking markers WL1975 and WL2282. From the first part of the population, 960 $F_3$ individuals, we identified 42 recombinants. These 42 recombinants were genotyped using the *Iw3*-cosegregating marker psp3000, and two recombination events were found between *Iw3* and *Xpsp3000*, which placed *Iw3* between *XWL2282* and *Xpsp3000*. With this result, we decided to screen the second part of the population, 2,400 $F_3$ individuals, using markers WL2282 and psp3000. Genotyping the whole population identified 30 recombinants. These recombinants were genotyped with other cosegregating markers, including fcp168, WL1967, and WL3096, and phenotyped, and their genotypes at the *Iw3* locus were validated by $F_4$ progeny analysis. All this effort localized the *Iw3* locus in a 0.135-cM interval delimited by marker loci *XWL3096* and *Xpsp3000*, 0.015 cM proximal to the former and 0.12 cM distal to the latter (Fig. 2c).

## Wax morphology

The near isogenic pair and the heterozygote derived from the same $F_5$ family were subjected to SEM observation of their wax morphology. The abaxial surface of the glumes of the *iw3iw3* homozygotes was covered with thick meshwork of wax tubes (Fig. 3a), but small wax particles were seen on the cuticle surface of the *Iw3Iw3* homozygotes (Fig. 3c). An intermediate pattern, low density wax meshwork consisting of short wax tubes, was observed in the *Iw3iw3* heterozygotes (Fig. 3b). This indicates that *Iw3* inhibits glaucousness formation through changing the wax crystal morphology and verifies that the glaucousness-inhibiting effect by *Iw3* is partial dominant in a dosage-dependent manner. The wax crystal morphology is determined by specific wax components or their combination, implying that *Iw3* perturbs the wax metabolism and further the glaucousness formation process.

## Wax composition

We profiled the glume wax composition of the NILs by GC–MS. Glume wax from *iw3*-NIL contains 93.8 % known and 6.2 % unknown wax species. Of the known wax species, primary alcohols account for 67.7 %, fatty acids for 15.4 %, β-diketone for 13.4 %, alkanes for 2.6 %, and a total of aldehyde, wax esters and phytosterols for <1 %. Compared to the *iw3*-NIL, total wax load reduced 30 % in the *Iw3*-NIL ($P = 0.01561$; Fig. 4a). Regarding the individual wax species, β-diketones were eliminated ($P = 0.00709$) and primary alcohols reduced 47 % ($P = 0.00032$), but alkanes increased fivefold ($P = 0.001$) and aldehydes increased >400-fold ($P = 0.00544$) in the *Iw3*-NIL (Fig. 4b). Although fatty acid content remained similar between the two NILs ($P = 0.32425$), variations were observed among the chain-length homologs. Compared to the *iw3*-NIL, *Iw3*-NIL showed a significant increase in $C_{18:1}$, $C_{20}$, $C_{22}$, $C_{24}$, and $C_{30}$ but a decrease in $C_{26}$ fatty acid content ($P < 0.00579$; Fig. 5a). Related with this, primary alcohol content increased ($P < 0.03483$) for all the homologs except the $C_{26}$ homolog, which reduced 99.3 % in the *Iw3*-NIL ($P = 0.00005$; Fig. 5b). Furthermore, *Iw3* also increased $C_{30}$ aldehyde ~400-fold ($P = 0.00544$; Fig. 5c) and $C_{29}$ alkane 8.5-fold ($P = 0.00059$; Fig. 5d).

## Transcriptional profiling of wax genes

To gain insights into molecular mechanism by which *Iw3* perturbs wax metabolism, we measured transcription of wax genes. Considering that *Iw3* changed the content of primary alcohol, aldehyde, and alkanes and chain-length distribution patterns in addition to depletion of β-diketone,

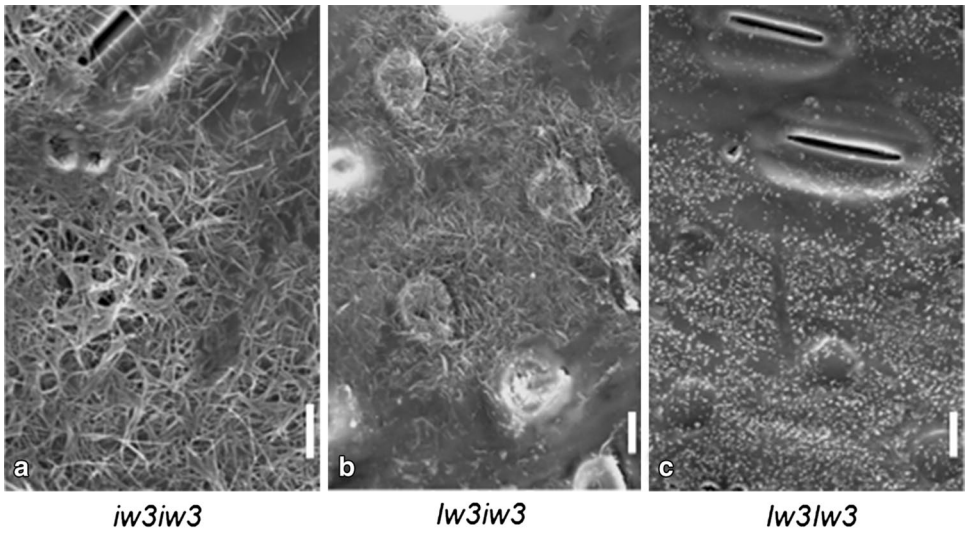


**Fig. 3** Electron micrographs of glume cuticle surfaces. Genotypes are indicated underneath each micrograph. The *scale bars* indicate 5 μm

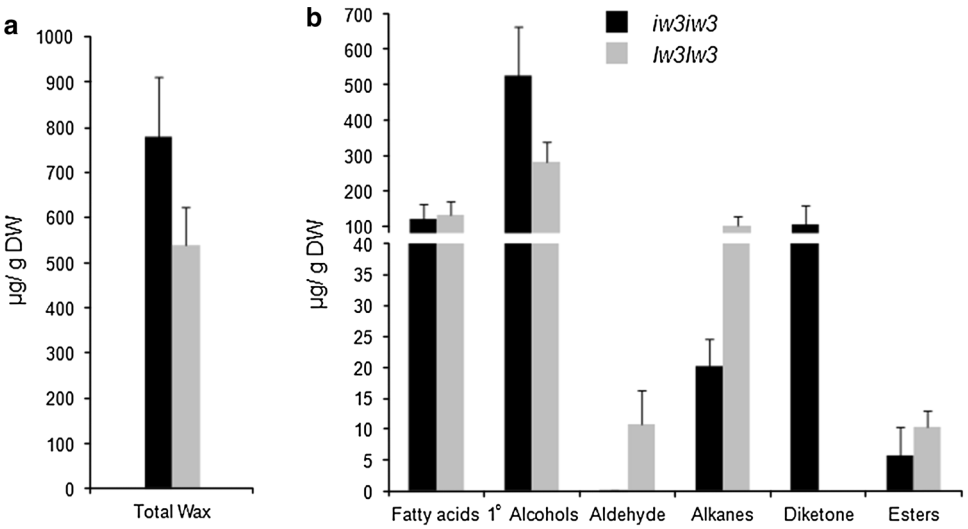


**Fig. 4** Wax composition of the *Iw3* NILs. (**a**) Total wax load of the glumes was measured by GC–MS. (**b**) Fatty acid, primary (1°) alcohol, aldehyde, alkane, β-diketone and wax ester content. The *numbers on the y*-axes indicate average content expressed as μg per g dried tissue (dry weight, DW). The *bars* indicate standard deviations of the means estimated from five biological replicates

we measured transcription of 53 wax genes from the acyl pathway: 17 for acyl elongation, 14 for acyl reduction and wax esterification, 17 for decarbonylation of fatty acids and hydroxylation of alkanes and five wax regulators (Supplementary Table 2 s). Of these 53 genes, transcription level of nine genes was significantly altered in *Iw3*-NIL compared to *iw3*-NIL. Fold changes of seven genes, *KCS2* and six *Cer4* homologs, are twofold or above (Fig. 6). No significant change was observed in the genes for decarbonylation (*Cer1* and *Cer3*), hydroxylation (*MHA*), and transcription regulation (Supplementary Table 2 s).

## Cuticle permeability

We analyzed *Iw3* effect on cuticle permeability by measuring the water loss and chlorophyll efflux rate of the NILs. Within the first hour after detachment, *Iw3*-NIL lost almost 68 % of water, 12 % higher than *iw3*-NIL did ($P = 0.01198$). From the third hour through the sixth hour, the water loss rate of *Iw3*-NIL significantly reduced as compared to *iw3*-NIL ($P < 0.03319$), and both NIL lines reached 100 % water loss at end of the seventh hour (Fig. 7a). The NILs also showed difference in chlorophyll leaching experiment. From second hour through the fifth hour of the treatment, *Iw3*-NIL showed a significantly higher chlorophyll leaching rate than *iw3*-NIL ($P < 0.04625$). No difference was observed after 6 h of treatment (Fig. 7b). There is no significant difference in water content and chlorophyll content between the glumes of NIL pair ($P > 0.40847$). This suggests that *Iw3* increased cuticle permeability.

## Discussion

In addition to its function in protection of plants from the abiotic and biotic stresses, cuticle also plays important

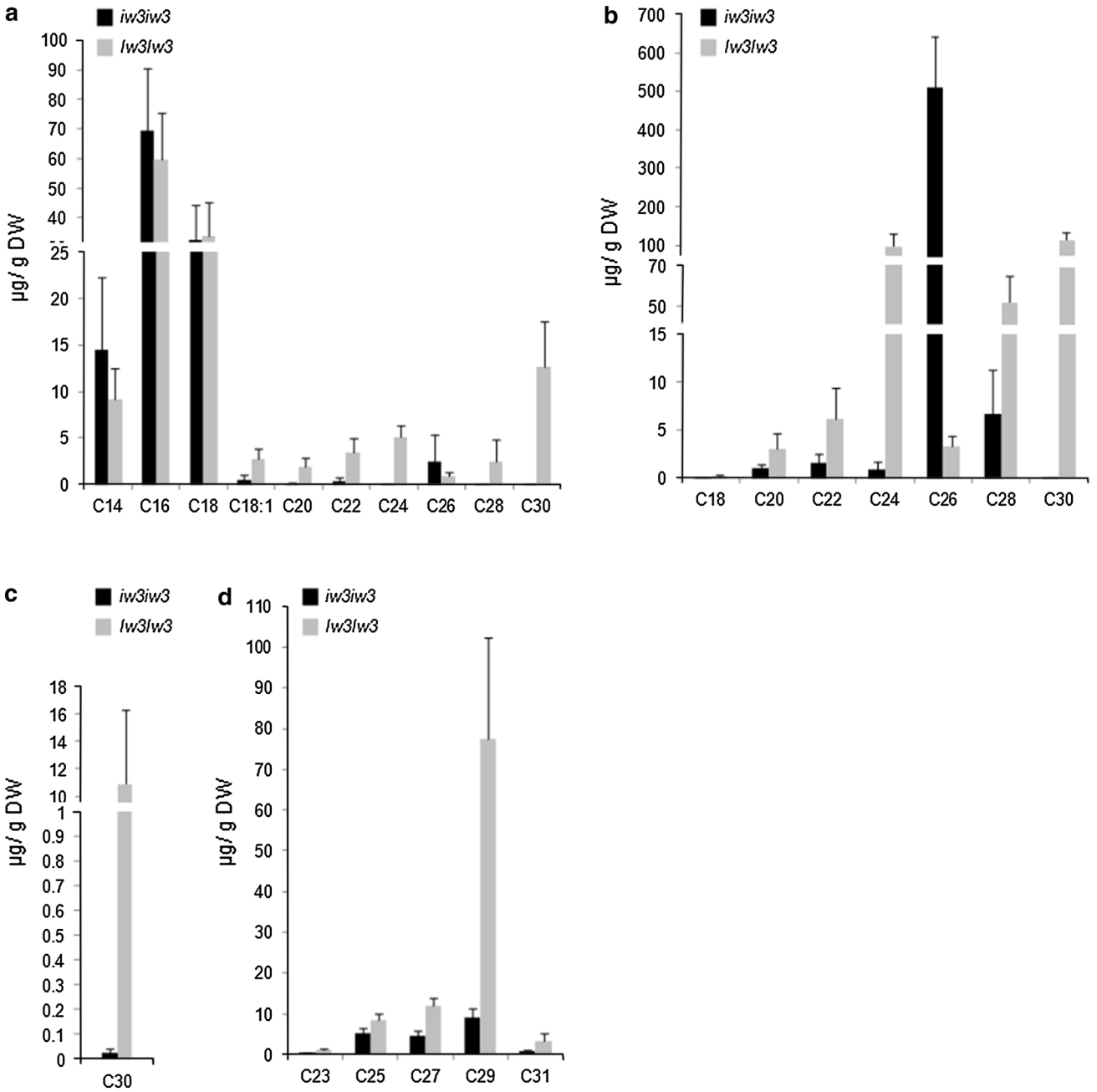


**Fig. 5** Homolog variation of major wax species. Carbon atom numbers of fatty acids (**a**), primary alcohols (**b**), aldehyde (**c**), and alkanes (**d**) are indicated on the *x*-axes. Their contents are indicated on *y*-axes as µg per g dried tissue. The *bars* indicate standard deviations of the means calculated from five biological replicates

roles in plant development. At the same time, cuticle deposition is regulated by developmental programs and affected by environmental cues. As a result, composition of the cuticular wax varies among different developmental stages and organs and under different water regimes (Kosma et al. 2009). A recent study in the model plant Arabidopsis found that transcription of several wax biosynthetic genes is regulated by an ABA-responsive transcription factor (Seo et al. 2011), which explains the environmental effect on wax metabolism (Seo and Park 2011). But the developmental regulation of wax biosynthesis is largely unknown. In wheat, glaucousness is only observed in the upper part of the adult plants. Of the five known wax loci in wheat, *Iw3* showed a unique expression pattern, i.e. glume-specific. In-depth investigation of the molecular mechanism of glaucousness inhibition by *Iw3* will provide us insights into

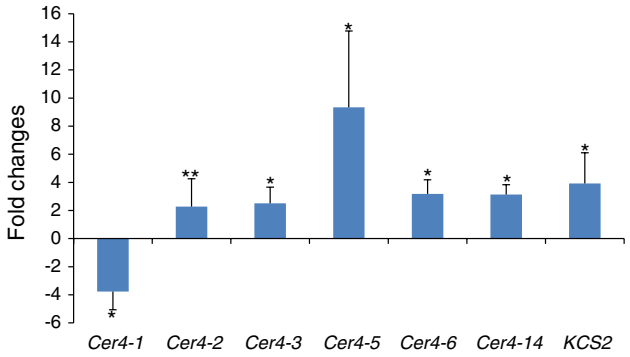


**Fig. 6** The expression of cuticular wax-related genes in the wheat glume of *Iw3*-NIL compared to *iw3*-NIL. Genes with two- or higher-fold changes are depicted, and expression data for all genes analyzed are listed in Supplementary Table 2 s. The *bars* represent standard deviations of the mean fold-changes of mRNA levels calculated from four biological replicates. *Asterisks* indicate that the difference is significant at $*P < 0.05$ or at $**P < 0.01$

how the wax metabolism is integrated into plant developmental programs. As an initial step of this effort, we localized the *Iw3* locus within a sub-cM interval, analyzed its effect on wax composition and morphology, cuticle permeability, and transcription of wax genes. These results enriched our understanding of the *Iw3* effect and paved way for eventual molecular identification and functional analysis of this glume glaucousness inhibitor.

## Perturbation of wax metabolism by the *Iw* genes

The most significant effect by *Iw3* is inhibition of glaucousness formation. Studies on other known wax genes indicated that failure to form glaucousness is due to depletion in β-diketones (Adamski et al. 2013; Bianchi and Figini 1986; Zhang et al. 2013). GC–MS profiling of the wax samples from the NILs showed that *Iw3* causes elimination of β-diketones from the glume wax (Fig. 5). In the sheath, β-diketones are the major wax component, accounting for 63 % of the total wax load. Reduction of β-diketones to 8 % in the *w1w2* double recessive line fails to form the meshwork of wax crystal morphology and glaucousness (Zhang et al. 2013). By contrast, glume wax had β-diketone content of 13 %, crystallized into the meshwork of wax tubes, and formed glaucousness. This suggests that β-diketone content is critical for wax crystal morphology and glaucousness formation with a threshold somewhere between 8 % and 13 %.

In addition to inhibition of β-diketone biosynthesis, like other *Iw* genes, *Iw3* also affects the acyl pathway. While eliminating β-diketones, *Iw1* and *Iw2* elevate primary alcohols, especially the $C_{26}$ homolog, but alkanes remain unchanged (Zhang et al. 2013). Opposite to *Iw1* and *Iw2*, however, *Iw3* reduced the primary alcohol, mainly $C_{26}$ homolog (Figs. 4b, 5b). *Iw3* also differs from *Iw1* and *Iw2* in altering the decarbonylation branch of the acyl pathway, i.e. increasing aldehyde and alkanes. All this suggests that *Iw3* employs a mechanism different from *Iw1* and *Iw2* in suppressing the β-diketone pathway.

Difference between mechanisms mediated by *Iw1*, *Iw2* and *Iw3* is also reflected in the expression patterns of wax genes. *Iw1* and *Iw2* changed the expression of 10 and 26 of genes in acyl elongation, reduction, decarbonylation, and transcription regulation, respectively (Zhang et al. 2013). We profiled transcription of 53 wax genes and found significant fold changes in nine genes functioning in acyl elongation and reduction, but none of 22 genes for the decarbonylation and regulation were affected (Fig. 6; Supplementary Table 2 s). *Iw2* and *Iw3* shared expression patterns in *Cer4-1*, *Cer4-3*, *Cer4-5*, *Cer4-6* and *KCS2* despite differences in the transcription levels. The elevated transcription of three *KCS* and five *Cer4* homologs by *Iw3* may contribute to the increase of $C_{28}$ and $C_{30}$ VLCFAs and

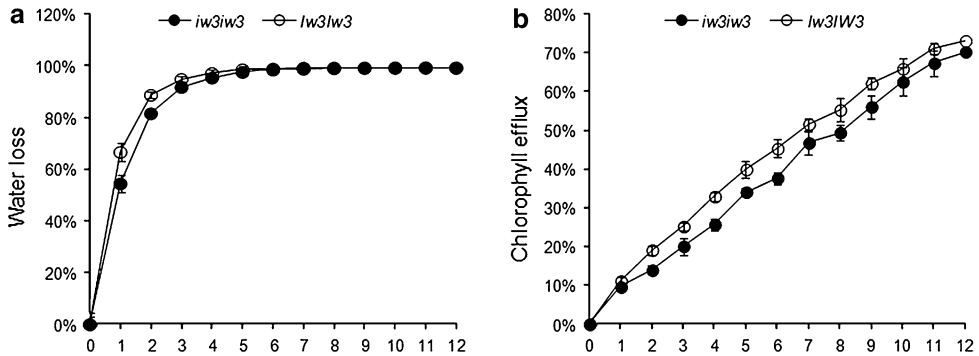


**Fig. 7** Cuticle permeability of the *Iw3* NILs. Cuticle permeability was evaluated by air drying at room temperature (**a**) and chlorophyll leaching in 80 % ethanol (**b**). The *numbers on the x-axes* represent hours of treatment. Water loss and chlorophyll leaching at each time point are represented on the *y*-axes as percentages of the total water content or total chlorophyll content in the tissue. The *bars* indicate standard deviations of the means calculated from eight biological replicates

alcohols, and downregulation of *Cer4-1* may be related to the overall reduction of primary alcohols, particularly the $C_{26}$ alcohol. The increase of aldehyde and alkanes could be due to a feed-forward effect of the increased fatty acid substrates or by other *Cer1* and/or *Cer3* homologs that were not included in our collection.

## Glaucousness and drought tolerance

Physiological studies in the late 20th century indicated that glaucousness in wheat can significantly reduce photosynthetic temperature (Jefferson et al. 1989; Richards et al. 1986), prevent pre-harvest sprouting (King and Wettstein-Knowles 2000), and increase WUE and yield in the rainfed condition (Johnson et al. 1983; Richards et al. 1986). More recently, however, experiments conducted in different water regimes reached different conclusions regarding effect of glaucousness on WUE. Experiments performed in Mexico, where no rainfall was received during the growing cycle, showed significant contribution of glaucousness to grain yield even in irrigated condition (Monneveux et al. 2004); but the experiment in UK, where rainfall and relative humidity were much higher, showed no effect (Adamski et al. 2013). This may suggest that the glaucousness effect on WUE is closely related with the growing environments, particularly rainfall, relative humidity, and temperature. Under the laboratory condition, our previous study on *Iw1* and *Iw2* indicated that the glaucousness-forming wax, β-diketones, reduced cuticle permeability, and that increase of acyl pathway products, primary alcohols and alkanes did not compensate loss of β-diketones (Zhang et al. 2013). In the present study, *Iw3* inhibited glaucousness and increased cuticle permeability in terms of water loss and chlorophyll leaching (Fig. 7). Biochemically, *Iw3* depleted β-diketone and reduced primary alcohols by half, although it increases aldehyde 400-fold and alkanes fivefold (Fig. 4b). The aldehyde and alkanes are more hydrophobic than primary alcohols, suggesting that the former has greater effect on water protection. Reduction in primary alcohols and increase in aldehyde and alkanes should have reduced the cuticle permeability in the *Iw3*-NIL. Therefore, the increased cuticle permeability in *Iw3*-NIL was caused by the loss of β-diketone although it is not the most abundant species in the glume wax. All this suggests that β-diketone is the major determinant of glaucousness formation and cuticle impermeability despite low abundance.

## Glaucousness inhibitor or producer?

Besides the differences in metabolite spectrum, *Iw3* differs from *Iw1* and *Iw2* in genetic mode. The glaucousness phenotype and SEM micrograph of the heterozygote indicated that the dominance of glaucousness-inhibiting effect mediated by *Iw3* is partial (Figs. 1, 3). An alternative explanation would be that the nonglaucousness is caused by a loss-of-function mutation of a glaucousness-forming gene, which has an additive effect on glaucousness intensity in a dosage-dependent manner. Peng et al. (2000) mapped a spike wax locus *Ws* to distal region of 1BS. It would be interesting to see if *Iw3* and *Ws* are allelic. In the present study, several closely linked markers including fcp168 and WL3096 are dominant, and no amplification was detected, possibly due to deletions, in the nonglaucous parent LDN-TDIC 1B. This may lend support to a hypothesis that *Iw3* could be a null or nonfunctional allele. However, direct evidence to discriminate these two scenarios whether *Iw3* is a glaucousness inhibitor or a nonfunctional allele of a glaucousness producer will eventually come from the comparison of DNA sequences of the *Iw3* and *iw3* alleles.

Currently no gene has been identified in the β-diketone pathway. Map-based cloning is a straightforward approach for the genes with unknown products. *Iw3* is located in the very distal portion of 1BS. The present research localized the *Iw3* locus within a 0.135-cM interval delimited by *Xpsp3000* and *XWL3096* (Fig. 2c). Because this genomic region is high in gene density and recombination rate (Qi et al. 2004), our sub-cM map will sever as the starting point for map-based cloning of *Iw3*. The colinear regions of wheat homeologous group-1 chromosomes carry numerous agriculturally important genes, including storage protein-coding genes *Gli1* and *Glu3* (Dubcovsky et al. 1997), and disease resistance gene *Lr21* (Huang et al. 2003), *Pm3* (Yahiaoui et al. 2004) and *Snn1* (Reddy et al. 2008), and insect resistance genes *H9*, *H10* and *H11* (Liu et al. 2005). As a result, this region is rich in the genomic resources, such as genetic and physical maps, molecular markers, and sequences. In addition, a 1BS-specific bacterial artificial chromosome (BAC) library (Janda et al. 2006) and chromosome survey sequences (wheatgenome.org) are available in wheat cultivar Chinese Spring, and a BAC-based physical map is under construction (wheatgenome.org). All these resources will facilitate the identification of *Iw3* candidate gene. Cloning of *Iw3* will shed light on β-diketone biosynthesis and developmental regulation of wax metabolism. Furthermore, we developed *Iw3* NILs. They are the ideal plant material for profiling the *Iw3*-dependent transcriptomes by RNA-seq, which will provide information of gene regulation network and *Iw3*-mediated crosstalks between the acyl and β-diketone pathways.

**Acknowledgments** We thank Dr. Justin Faris for providing seeds of LDN, LDN-TDIC 1B, and the RSL population. This research is supported by South Dakota Agricultural Experiment Station (Brookings, SD) and South Dakota Wheat Commission (Pierre, SD). JW's stay in US is supported by a fellowship from the Ministry of Education of the People's Republic of China.

**Conflict of interest** The authors declare that they have no conflict of interest.

## References


Adamski NM, Bush MS, Simmonds J, Turner AS, Mugford SG, Jones A, Findlay K, Pedentchouk N, von Wettstein-Knowles P, Uauy C (2013) The Inhibitor of wax 1 locus (*Iw1*) prevents formation of beta- and OH-beta-diketones in wheat cuticular waxes and maps to a sub-cM interval on chromosome arm 2BS. Plant J 74:989–1002

Bennett D, Izanloo A, Edwards J, Kuchel H, Chalmers K, Tester M, Reynolds M, Schnurbusch T, Langridge P (2012) Identification of novel quantitative trait loci for days to ear emergence and flag leaf glaucousness in a bread wheat (*Triticum aestivum* L.) population adapted to southern Australian conditions. Theor Appl Genet 124:697–711

Bernard A, Joubès J (2013) Arabidopsis cuticular waxes: advances in synthesis, export and regulation. Prog Lipid Res 52:110–129

Bianchi G (1995) Plant waxes. In: Hamilton RJ (ed) Waxes: chemistry, molecular biology and functions. The Oily Press, Dundee, pp 175–222

Bianchi G, Figini ML (1986) Epicuticular waxes of glaucous and nonglaucous durum wheat lines. J Agric Food Chem 34:429–433

Cheesbrough TM, Kolattukudy PE (1984) Alkane biosynthesis by decarbonylation of aldehydes catalyzed by a particulate preparation from *Pisum sativum*. Proc Natl Acad Sci USA 81:6613–6617

Devos KM, Bryan GJ, Collins AJ, Stephenson P, Gale MD (1995) Application of two microsatellite sequences in wheat storage proteins as molecular markers. Theor Appl Genet 90:247–252

Dubcovsky J, Echaide M, Giancola S, Rousset M, Luo MC, Joppa LR, Dvorak J (1997) Seed-storage-protein loci in RFLP maps of diploid, tetraploid, and hexaploid wheat. Theor Appl Genet 95:1169–1180

Greer S, Wen M, Bird D, Wu X, Samuels L, Kunst L, Jetter R (2007) The cytochrome P450 enzyme CYP96A15 is the midchain alkane hydroxylase responsible for formation of secondary alcohols and ketones in stem cuticular wax of Arabidopsis. Plant Physiol 145:653–667

Huang L, Brooks SA, Li W, Fellers JP, Trick HN, Gill BS (2003) Map-based cloning of leaf rust resistance gene *Lr21* from the large and polyploid genome of bread wheat. Genetics 164:655–664

Janda J, Safár J, Kubaláková M, Bartos J, Kovárová P, Suchánková P, Pateyron S, Číhalíková J, Sourdille P, Simková H, Faivre-Rampant P, Hribová E, Bernard M, Lukaszewski A, Dolezel J, Chalhoub B (2006) Advanced resources for plant genomics: a BAC library specific for the short arm of wheat chromosome 1B. Plant J 47:977–986

Jefferson PG, Johnson DA, Asay KH (1989) Epicuticular wax production, water status and leaf temperature in Triticeae range grasses of contrasting visible glaucousness. Can J Plant Sci 69:513–519

Johnson DA, Richards RA, Turner NC (1983) Yield, water relations, gas exchange, and surface reflectances of near-isogenic wheat lines differing in glaucousness. Crop Sci 23:318–325

Joppa LR, Cantrell RG (1990) Chromosomal location of genes for grain protein content of wild tetraploid wheat. Crop Sci 30:1059–1064

King RW, Pv Wettstein-Knowles (2000) Epicuticular waxes and regulation of ear wetting and pre-harvest sprouting in barley and wheat. Euphytica 112:157–166

Kosambi DD (1944) The estimation of map distances from recombination values. Ann Eugen 12:172–175

Kosma DK, Bourdenx B, Bernard A, Parsons EP, Lu S, Joubes J, Jenks MA (2009) The impact of water deficiency on leaf cuticle lipids of Arabidopsis. Plant Physiol 151:1918–1929

Lander ES, Green P, Abrahamson J, Barlow A, Daly MJ, Lincoln SE, Newberg LA (1987) MAPMAKER: an interactive computer package for constructing primary genetic linkage maps of experimental and natural populations. Genomics 1:174–181

Large EC (1954) Growth stages in cereals illustration of the feekes scale. Plant Pathol 3:128–129

Lee SB, Suh MC (2013) Recent advances in cuticular wax biosynthesis and its regulation in Arabidopsis. Mol Plant 6:246–249

Li W, Huang L, Gill BS (2008) Recurrent deletions of puroindoline genes at the grain hardness locus in four independent lineages of polyploid wheat. Plant Physiol 146:200–212

Liu XM, Fritz AK, Reese JC, Wilde GE, Gill BS, Chen MS (2005) *H9*, *H10*, and *H11* compose a cluster of Hessian fly-resistance genes in the distal gene-rich region of wheat chromosome 1AS. Theor Appl Genet 110:1473–1480

Liu Q, Ni Z, Peng H, Song W, Liu Z, Sun Q (2006) Molecular mapping of a dominant non-glaucousness gene from synthetic hexaploid wheat (*Triticum aestivum* L.). Euphytica 155:71–78

Livak KJ, Schmittgen TD (2001) Analysis of relative gene expression data using real-time quantitative PCR and the $2^{-\Delta\Delta CT}$ method. Methods 25:402–408

Lolle SJ, Berlyn GP, Engstrom EM, Krolikowski KA, Reiter WD, Pruitt RE (1997) Developmental regulation of cell interactions in the Arabidopsis fiddlehead-1 mutant: a role for the epidermal cell wall and cuticle. Dev Biol 189:311–321

Monneveux P, Reynolds MP, González-Santoyo H, Peña RJ, Mayr L, Zapata F (2004) Relationships between grain yield, flag leaf morphology, carbon isotope discrimination and ash content in irrigated wheat. J Agron Crop Sci 190:395–401

Nelson JC, Deynze AE, Sorrells ME, Autrique E, Lu YH, Merlino M, Atkinson M, Leroy P (1995) Molecular mapping of wheat. Homoeologous group 2. Genome 38:516–524

Peng J, Korol AB, Fahima T, Röder MS, Ronin YI, Li YC, Nevo E (2000) Molecular genetic maps in wild emmer wheat, *Triticum dicoccoides*: genome-wide coverage, massive negative interference, and putative quasi-linkage. Genome Res 10:1509–1531

Pennisi E (2008) Plant genetics. The blue revolution, drop by drop, gene by gene. Science 320:171–173

Pighin JA, Zheng H, Balakshin LJ, Goodman IP, Western TL, Jetter R, Kunst L, Samuels AL (2004) Plant cuticular lipid export requires an ABC transporter. Science 306:702–704

Reddy L, Friesen TL, Meinhardt SW, Chao S, Faris JD (2008) Genomic analysis of the *Snn1* locus on wheat chromosome arm 1BS and the identification of candidate genes. Plant Genome J 1:55

Richards RA, Rawson HM, Johnson DA (1986) Glaucousness in wheat: its development and effect on water-use efficiency, gas exchange and photosynthetic tissue temperature. Aust J Plant Physiol 13:465–473

Röder MS, Korzun V, Wendehake K, Plaschke J, Tixier MH, Leroy P, Ganal MW (1998) A microsatellite map of wheat. Genetics 149:2007–2023

Samuels L, Kunst L, Jetter R (2008) Sealing plant surfaces: cuticular wax formation by epidermal cells. Ann Rev Plant Biol 59:683–707

Seo PJ, Park CM (2011) Cuticular wax biosynthesis as a way of inducing drought resistance. Plant Signal Behav 6:1043–1045

Seo PJ, Lee SB, Suh MC, Park MJ, Go YS, Park CM (2011) The MYB96 transcription factor regulates cuticular wax biosynthesis under drought conditions in Arabidopsis. Plant cell 23:1138–1152

Shepherd T, Wynne Griffiths D (2006) The effects of stress on plant cuticular waxes. New Phytol 171:469–499

Shimazaki K, Doi M, Assmann SM, Kinoshita T (2007) Light regulation of stomatal movement. Ann Rev Plant Biol 58:219–247

Simmonds JR, Fish LJ, Leverington-Waite MA, Wang Y, Howell P, Snape JW (2007) Mapping of a gene (*Vir*) for a non-glaucous,

viridescent phenotype in bread wheat derived from *Triticum dicoccoides*, and its association with yield variation. Euphytica 159:333–341

Somers DJ, Isaac P, Edwards K (2004) A high-density microsatellite consensus map for bread wheat (*Triticum aestivum* L.). Theor Appl Genet 109:1105–1114

Tsunewaki K, Ebana K (1999) Production of near-isogenic lines of common wheat for glaucousness and genetic basis of this trait clarified by their use. Genes Genet Syst 74:33–41

Tulloch AP (1973) Composition of leaf surface waxes of *Triticum* species: variation with age and tissue. Phytochem 12:2225–2232

Vioque J, Kolattukudy PE (1997) Resolution and purification of an aldehyde-generating and an alcohol-generating fatty acyl-coa reductase from pea leaves (*Pisum sativum* L.). Arch Biochem Biophys 340:64–72

von Wettstein-Knowles P (1995) Biosynthesis and genetics of waxes. In: Hamilton RJ (ed) Waxes: chemistry, molecular biology and functions. The Oily Press Dundee, UK, pp 91–129

von Wettstein-Knowles P (2012) Plant Waxes eLS. Wiley, New York, pp 1–11

Qi LL, Echalier B, Chao S, Lazo GR, Butler GE, Anderson OD, Akhunov ED, Dvorak J, Linkiewicz AM, Ratnasiri A, Dubcovsky J, Bermudez-Kandianis CE, Greene RA, Kantety R, LaR CM, Munkvold JD, Sorrells SF, Sorrells ME, Dilbirligi M, Sidhu D, Erayman M, Randhawa HS, Sandhu D, Bondareva SN, Gill KS, Mahmoud AA, Ma X-F, Miftahudin, Gustafson JP, Wennerlind EJ, Nduati V, Gonzalez-Hernandez JL, Anderson JA, Peng JH, Lapitan NLV, Hossain KG, Kalavacharla V, Kianian SF, Pathan MS, Zhang DS, Nguyen HT, Choi D-W, Close TJ, McGuire PE, Qualset CO, Gill BS (2004) A chromosome bin map of 10,000 expressed sequence tag loci and distribution of genes among the three genomes of polyploid wheat. Genetics 168:701–712

Yahiaoui N, Srichumpa P, Dudler R, Keller B (2004) Genome analysis at different ploidy levels allows cloning of the powdery mildew resistance gene Pm3b from hexaploid wheat. Plant J 37:528–538

Zhang Z, Wang W, Li W (2013) Genetic interactions underlying the biosynthesis and inhibition of b-diketones in wheat and their impact on glaucousness and cuticle permeability. PLoS One 8:e54129